Spectroscopy of XeF in Ar and Ne matrices

G. Zerza, G. Sliwinski,[a] N. Schwentner
Institut für Experimentalphysik, Freie Universität Berlin, Arnimallee 14, D 14195 Berlin, Germany

G. J. Hoffman,[b] D. G. Imre,[c] and V. A. Apkarian
Department of Chemistry, University of California, Irvine, California 92717

(Received 22 July 1993; accepted 19 August 1993)

Spectroscopic constants for the $B\,^2\Sigma^+$ and $C\,^2\Pi$ charge transfer states of XeF in Ar and Ne matrices are derived from vibrational progressions in excitation and emission spectra. Polarization effects on the T_e values are discussed and Rittner potentials are fitted to the constants. Emissions at 389 and 411 nm in Ne and Ar, respectively, are attributed to a distorted B state denoted as B^* with a strong red shift of T_e and an about 30% larger ω_e. B^* is assigned to a XeF center with an additional F atom which can be a precursor to XeF_2 according to a comparison with Xe_2F spectra and the concentration dependence of the intensities. The B^* vibrational bands display two well resolved fine structure progressions with a common ω_e of $\sim 60\ cm^{-1}$ in Ar and Ne which is close to the maximum matrix phonon density and one with $30\ cm^{-1}$ in Ne and $15\ cm^{-1}$ in Ar. A reversible change in the Ne fine structure pattern with temperature can be correlated to a face-centered-cubic–hexagonal close-packed (fcc–hcp) phase transition.

I. INTRODUCTION

Laser applications stimulated intense experimental and theoretical investigations of the rare gas halides, in general, and XeF, in particular.[1] The $C \leftarrow X$, $B \leftarrow X$, $D \leftarrow X$, $C \rightarrow A$, $B \rightarrow X$, and $D \rightarrow X$ transitions were characterized in 1976 by Ault and Andrews[2] and by Goodman and Brus[3] in rare gas matrices. Molecular constants given in Table I were derived from absorption, emission, and excitation spectroscopy. A controversy in the gas phase about the relative positions of the close lying B and C states was resolved and good spectroscopic data of the X, C, B, and D states of the free molecule are now available.[4–6] The parameters are summarized in Table I. Calculations of the potential energy surfaces, dipole moments, transition moments, and lifetimes[7] confirmed that the X and A ground states are predominantly covalent, whereas the excited C, B, and D states are ionic. The covalent and ionic $^2\Sigma^+$ states (X and B) are more strongly mixed than the two $^2\Pi$ states (A and C). The mixing causes a crossing between the ionic B and C states and it stabilizes the X state by a fractional ionic character of 0.094. The fractional ionic characters result in dipole moments of -1.2 and -11.6 D for the X and B states, respectively, at the bond length of the B state.[7] The early matrix studies[2,3] were helpful in clarifying the electronic structure of the XeF molecule. Now with reliable free molecule data at hand, XeF can serve as a prototype molecule to study polarization effects for transitions from weakly bound covalent to strongly bound ionic states. For this purpose, shifts of electronic transition energies, vibrational constants, and anharmonicities will be investigated in this paper for Ne and the more polarizable Ar matrices.

A renewed interest in the spectroscopic properties of XeF in Ar and Ne arises in part from the successful application of these systems for high gain solid state excimer lasers working on the $D \rightarrow X$, $B \rightarrow X$, and $C \rightarrow A$ transitions.[8–14] Inspection of the existing matrix work reveals that well-resolved vibrational progressions in excitation spectra were reported only for the $D \leftarrow X$ transition in Ne,[3] whereas for $B \leftarrow X$ and $C \leftarrow X$ in Ar and Ne, only weakly modulated absorption spectra, which do not allow clear assignments, were published.[2] Excitation at wavelengths longer than 350 nm gave no emission in Ne and only a weak emission in Ar.[3] In addition, only the assignment of the $D \rightarrow X$ and $B \rightarrow X$ emission was unambiguous in the early work,[3] whereas, e.g., the 536 nm band in Ar matrix was attributed to a different species due to the varying intensity ratios relative to the B transitions for different preparation conditions.[3] Recent systematic investigations of XeF in Ar and Kr matrices for laser applications[8–14] and with respect to the photochemical processes involved in the XeF formation[15–20] clarified the assignment of the 286, 411, and 540 nm emission bands in Ar to the $D \rightarrow X$, $B \rightarrow X$, and $C \rightarrow A$ transitions. Nevertheless, the new excitation spectra presented in this paper will confirm the original idea that the B–X and C–A emissions in Ar and also in Ne originate from two quite distinct species or sites. Moreover, the vibrational assignments, phonon sidebands, contributions of hot emission, new $B \rightarrow A'$ transition, and coupling between the B and C states as well as static and temperature induced site effects will be treated.

II. EXPERIMENT

In the case of Ne matrices, a premixed gas with a typical concentration of 1:1:2000 of F_2:Xe:Ne was condensed on a quartz substrate. The substrate was cooled by a liquid He flow cryostat to temperatures between 5 and 12 K. Doped Ne crystals were also grown in a quartz box.[18] These samples gave similar results, but the growth process

[a] Permanent address: Polish Academy of Sciences, IF-FM, Fiszera 14, PL 80-952 Gdansk.
[b] Present address: College of William and Mary, Williamsburg, VA 23187-8795.
[c] Present address: Chemical Sciences Division, Brookhaven National Laboratory, Upton, NY 11973.

 0021-9606/93/99(11)/8414/10/$6.00

TABLE I. A comparison of the spectroscopic constants T_e, ω_e, and $\omega_e x_e$ (in cm^{-1}) of XeF for the ground state $X\,^2\Sigma^+$ and the $B\,^2\Sigma^+$, $C\,^2\Pi$, and $D\,^2\Pi$ charge transfer states in the gas phase and in Ar and Ne matrices. B^* is a distorted B state (see the text).

		T_e	ω_e	$\omega_e x_e$	Footnote
X	Gas	0	225	10.9	a
	Ne	0	247	10.2	b
	Ar	0	205	10.	
B	Gas	28 811	309	1.51	a
	Ne	28 303	301	2	
	Ar	27 210			c
C	Gas	28 023	346	2.2	d
	Ne	27 544	301	2	
	Ar	26 200	300		c
D	Gas	38 051	350	1.9	a
	Ne	37 550	330		b
	Ar	36 000	320		e
B^*	Gas	28 811	309	1.51	a
	Ne	26 071	446	14.1	
	Ar	24 566	424	7.5	

[a]Reference 5.
[b]Reference 3.
[c]Estimate based on broadbands in Fig. 4.
[d]Reference 6.
[e]Estimate from Ref. 2.

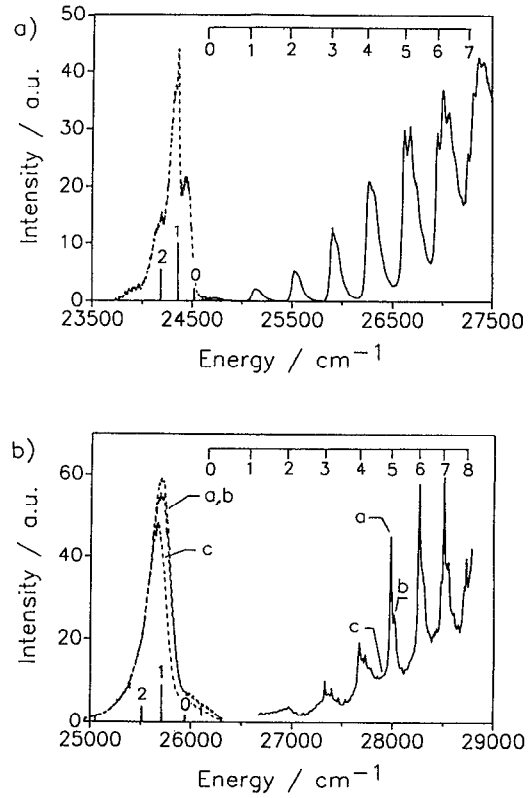

FIG. 1. Excitation spectra (solid lines) and emission spectra of the B^*–X transition (see the text) in (a) Ar and (b) Ne matrices. Temperature for Ne was 10 K and *a*, *b*, and *c* denote excitation energies for the corresponding emission spectra.

of Ne solids was rather sensitive to the thermal contacts and only results from film experiments will be presented for Ne. The F_2 molecules were dissociated with a XeCl excimer laser (308 nm) and the growth of the XeF content was monitored by the XeF fluorescence. Excitation spectra and emission spectra were taken after saturating the dissociation with an excimer pumped dye laser. The fluorescence was dispersed with a 0.5 m Minuteman monochromator (1200 lines/mm grating). Emission spectra were recorded with a spatially resolving reticon system. For excitation spectra, the dispersed fluorescence was detected by an XP2020 photomultiplier and a boxcar integrator and averager system.

In the case of Ar matrices, doped crystals were grown in a quartz box from a premixed gas with a typical concentration of 1:1:3000 of F_2:Xe:Ar. The box was cooled by a closed cycle refrigerator to temperatures between 15 and 25 K. Excitation and emission spectra were taken after a photolysis cycle similar to the Ne case with a dye laser by dispersing the fluorescence with a 0.25 m monochromator and recording with a reticon system (emission spectra) or a photomultiplier and a boxcar system (excitation spectra). Hot fluorescence from the B state was recorded with a 1 m double monochromator to improve the stray light rejection.

III. RESULTS

It will be argued below that the matrix emission which is strongly related to the gas phase B–X transition originates from a complex center containing XeF and most probably an additional F atom. We will denote this state as B^* to distinguish it from the ordinary B state of the isolated XeF molecule which shows only C emission.

A. $B^* \rightarrow X$ emission and excitation spectra

1. Ar matrix

The emission of XeF in Ar around 411 nm was attributed by all authors[2,3,8] to the $B \rightarrow X$ transition based on its spectral shape, the measured lifetime of $\sim$6 ns, and the observed parallel polarization. An emission spectrum for excitation of $v'=0$ and an excitation spectrum for an emission wavelength of 411 nm (24 331 cm^{-1}) are compared in Fig. 1(a). The comparison allows an unambiguous assignment of the vibrational progression in the excitation spectrum and the energies are listed in Table II. The vibrational bands are well resolved in strong contrast to the previously published absorption spectrum[2] which only shows a weak modulation. A fine structure can be identified in the bands, typical examples of which are shown on an expanded scale in Fig. 2. The spacings are of the order of 10–15 cm^{-1} and only partially resolved for $v'=1$–4. A longer, more strongly modulated progression with a larger spacing of 55–60 cm^{-1} shows up for $v'=5$–7. The energies of the fine structures are listed, relative to the first maximum in Table III. The anharmonicity in the lower members can be influenced by the changes in the fine structure. The low energetic onsets which could be close to the zero phonon lines are therefore included in Table II and yield values of

TABLE II. Energies (in cm^{-1}) of vibrational bands in excitation spectra of B^* emission. (First and third rows) lowest energetic maximum (or shoulder) in Ar and Ne matrices (10 K), respectively; (second row) low energy onset in Ar. ΔG values are in brackets.

v'		Ar	Ne
0	24 702(408)	24 654(409)	26 171(407)
1	25 110(398)	25 063(402)	26 578(387)
2	25 508(391)	25 463(390)	26 965(366)
3	25 899(369)	25 853(367)	27 331(338)
4	26 268(349)	26 220(352)	27 669(316)
5	26 617(333)	26 572(345)	27 985(279)
6	26 950(300)	26 917(316)	28 264(245)
7	27 250	27 233	28 509(222)
8			28 731

TABLE III. Fine structure (in cm^{-1}) in the vibrational bands of the excitation spectra of B^* emission in the Ar matrix at 4 K and in the Ne matrix at 10 K.

v'	Ar	Ne
1	14	...
2	16	...
3	14	35, 65, 100, 135, 155, 200, 225
4	14, 54	30, 60, 100, 120, 190
5	59, 120	30
6	60, 120, 170	30
7	60, 115, 162	30, 70

$\omega_e' = 424\ cm^{-1}$ and $\omega_e x_e'$ of 7.5 cm^{-1} and $T_e = 24\ 655\ cm^{-1}$ (Table I). To rule out any contributions from hot emission, the $v'=0$ excitation was chosen for the emission spectrum in Fig. 1(a). An assignment of the maxima of the four observed bands to a vibrational progression yields a rather irregular anharmonicity (Table IV) with a spacing of 95 cm^{-1} between $v''=0$ and 1, and of 160 and 260 cm^{-1} for the higher bands. Since the line shape of the 0–0 and 0–1 band is very different, we tried to obtain a more regular progression from the blue edge of the bands (Table IV) which should be closer to the zero phonon lines. This progression is indeed regular, and ω_e and $\omega_e x_e$ values of 205 and 10 cm^{-1} are derived for the electronic ground state (Table I). They are not too far from the gas phase values, but the variations in the line shapes of the bands are already an indication for a strong distortion of the molecule at least in the excited electronic state. A comparison of the 0–0 transitions from the onsets of the bands in excitation and emission reveals a Stokes shift of 114 cm^{-1} and indicates that the zero phonon line of the emission band is still further to the blue of the observed onset. Thus a strong structural relaxation is involved in the excited state. A more precise determination of the zero phonon transition is hampered by the unknown inhomogeneous broadening of the bands.

Excitation of higher vibrational levels leads to hot fluorescence from $v'=1$ and $v'=2$ (Fig. 3). The assignment of the 1–0, 1–1, 2–0, and 2–1 bands is obvious, but the line shapes differ and the positions of the maxima evidence the irregular progressions. Consistent ω_e and ω_e' values can be derived only for the high energetic onsets of the bands (Table IV). The assignment of the hot bands at 24 870 and 24 680 cm^{-1} to 0–0 and 0–1 transitions in Ref. 2 has to be corrected according to our excitation spectra.

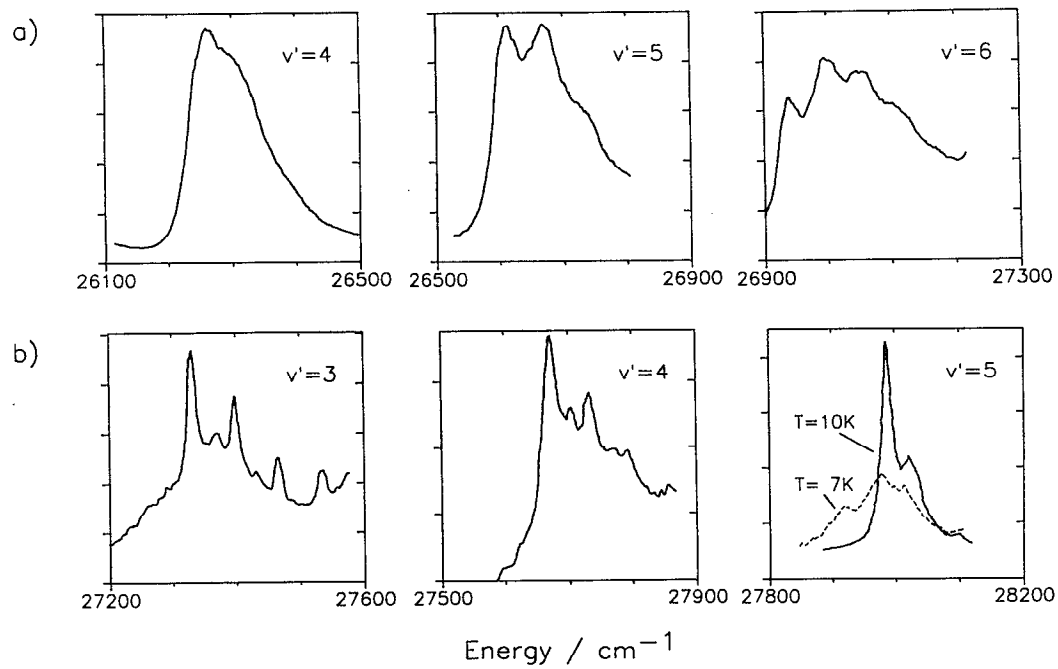

FIG. 2. Examples of vibrational bands with fine structure from the excitation spectra in Fig. 1 on an expanded scale for (a) Ar and (b) Ne. For Ne and $v'=5$, the reversible change for $T=10$ and 7 K is shown.

TABLE IV. Energies (in cm^{-1}) of $B^*(v') \rightarrow X(v'')$ emission bands in the Ar matrix for excitation of $v'=0$, 1, and 2. (Top) position of maxima; (bottom) position of high energetic onset. ΔG values are in brackets.

v'/v''	0	1	2	3
0	24 455 (95)	24 360 (160)	24 200 (260)	23 940
	(405)	(325)		
1	24 860 (175)	24 685		
	(440)	(485)		
2	25 300 (130)	25 170		
0	24 540 (185)	24 355 (165)	24 190 (152)	24 038
	(410)	(410)		
1	24 950 (185)	24 465		
	(405)	(405)		
2	25 355 (185)	25 170		

An analysis of the hot emission with respect to the relaxation dynamics is presented in Ref. 21.

2. Ne matrix

The B^*–X transition in Ne matrix has not been identified definitely in Ref. 3 because the band at 389 nm had the expected lifetime and transition energy, but a width of only 260 cm^{-1} and no vibrational structure as in Ar. We observe the same emission band [Fig. 1(b)] and attribute it to the B^*–X transition because its excitation spectrum [Fig. 1(b)] is quite similar to that of the B^*–X transition in Ar [Fig. 1(a)]. The only difference is the blue shift due to the smaller polarization energy of the ionic B^* state in the less polarizable Ne matrix. The unusual Franck–Condon envelope in emission should be attributed to the distorted structure of the center, which is also responsible for the complex phonon contours in the Ar matrix. The preparation dependent sideband in emission mentioned in Ref. 3 showed up in our experiments only in a Ne crystal, but not in the doped Ne films and will not be discussed in the following: the spacings between the zero phonon lines of the vibrational bands in the excitation spectra [Fig. 1(b) and Table II] result in values for ω_e' and $\omega_e x_e'$ of 446 and 14.1 cm^{-1}, respectively (Table I). Extrapolation from the first detected band at 26 578 cm^{-1} to lower energies leads to the vibrational numbering given in Fig. 1(b) and Table II. Each vibrational band has a characteristic fine structure which is displayed on an expanded scale in Fig. 2(b) and listed in Table III. For $v'=3$ and 4, two progressions with alternating intensities and energies of 30–35 and 60–65 cm^{-1} are clearly distinguished. The 65 cm^{-1} fine structure dies out for $v' \geqslant 5$. The fine structure is temperature dependent, and until now, results for the high temperature limit ($T \approx 10$ K) have been described. Lowering the temperature to 7 K causes a reduction in the sharp maxima and an additional band shifted by 60 cm^{-1} to lower energy appears, as is exemplified for $v'=5$ in Fig. 2(b). The changes are reversible in one sample, but the intensity ratios of the variations differ from sample to sample. The reversibility suggests that the modifications are due to a phase transition of the surrounding Ne matrix from face-centered cubic to hexagonal close-packed (fcc to hcp) in raising the temperature. Such a phase transition was previously identified in this temperature range.[22] The assumption of two different local structures is also supported by the emission spectra which are identical for excitation in the maxima *a* and *b* of $v'=5$ [Fig. 2(b)] (high temperature site), but show a small red shift [Fig. 1(b)] for excitation in band *c* which belongs to the low temperature site. A deconvolution of the emission spectrum into its vibrational components is problematic due to the complex band shapes caused by electron phonon coupling. With the information on the $B(0) \leftarrow X(0)$ band, a superposition of strongly phonon broadened $v''=0$, 1, 2, 3 bands as suggested by the stick diagram in Fig. 1(b) is most probable. The width of the phonon broadening in Ar [Fig. 1(a)] is at least 100 cm^{-1}. Increasing it in Ne to about 200 cm^{-1} leads to an overlap of the zero phonon lines in excitation and emission. This linewidth is also compatible with the overall half-width of 260 cm^{-1} of the emission spectrum and with its line shape if the Franck–Condon factor of the 0–0 emission is reduced in comparison to the Ar case. The overall width in Ar is only 300 cm^{-1}.

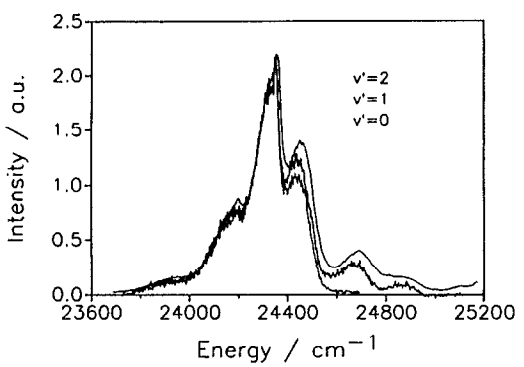

FIG. 3. Emission spectrum of B^* in Ar for excitation of $v'=0$, 1, and 2 shows fluorescence from $v'=0$ and hot bands from $v'=1$ and 2.

B. C–A emission and excitation spectra

In the Ar matrix, a broad emission in the green, centered at 536 nm, was observed by us [Fig. 4(a)] and in all other experiments.[2,3,8] The assignment to $B \rightarrow A$ (Ref. 2) was rejected by Goodman and Brus according to the lifetime ($\tau = 120 \pm 5$ ns) and polarization, and the emission was attributed to another species. The present assignment to the $C\ 3/2 \rightarrow A\ 3/2$ transition[8] is in accord with the lifetime, the polarization, and the width due to the repulsive A state.[23] The shift from the gas phase emission wavelength of 460 to 536 nm in Ar results from solvation of the ionic C state. The same arguments hold for the broad 483 nm emission in Ne [Fig. 4(b)] with a lifetime of about 100 ns, which has been observed, but not assigned by Goodman and Brus. Therefore it is also attributed to the $C \rightarrow A$ transition and the wavelength lies between the gas phase value and the Ar matrix values due to the weaker polarizability of Ne.

The excitation spectrum of the 483 nm band in Ne shows a very weak vibrational progression of three broad bands in the energy range from 27 500 to 28 500 cm^{-1}

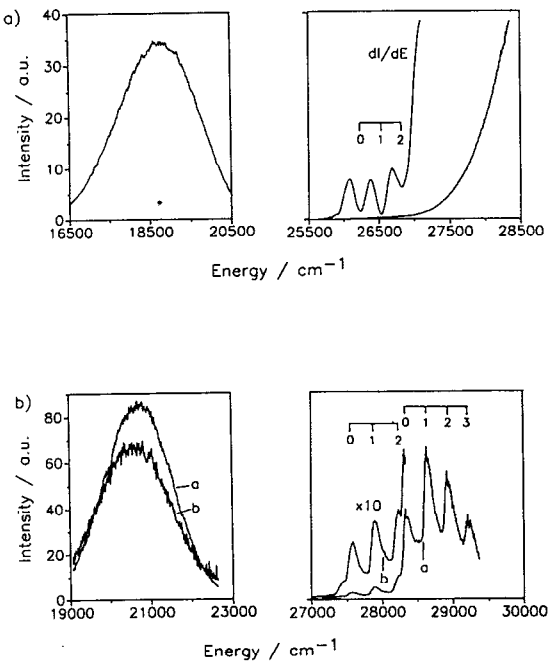

FIG. 4. *C–A* emission spectra (left-hand side) and the corresponding excitation spectra (right-hand side) in (a) Ar and (b) Ne matrices. A differentiated spectrum for Ar shows the weak modulations on the excitation spectrum and excitation at (a) and (b) in Ne yields the different emission spectra (a) and (b).

[Fig. 4(b) and Table V] followed by a second progression at higher energies with a factor of about 10 larger intensities. The only states that can be reached from the ground state in this energy range are the B and C states. The intensity ratio of 1:10 corresponds quite well to the 1:9 theoretical ratio of the C:B oscillator strength[7] and to the ratio of the experimental lifetimes, suggesting that the weak bands belong to the C state and the strong bands to the B state. The prompt onset and the broad envelope indicate that also the 0–0 vibrational band is observed yielding the vibrational numbering in Fig. 4(b) and Table V. The T_e, ω_e, and $\omega_e x_e$ values given in Table I were derived from the maxima in the excitation bands. The large width of the bands, typically 150 cm^{-1}, originates mainly from homogeneous multiphonon broadening, but it also contains an inhomogeneous contribution. This is evident from a shift in the $C \rightarrow A$ emission spectrum of the order of 100 cm^{-1} for different excitation energies (a and b) in Fig. 4(b).

TABLE V. Energies (in cm^{-1}) of the maxima in the excitation spectra of the $C \rightarrow A$ emission in Ar and Ne matrices representing $C \leftarrow X$ and $B \leftarrow X$ vibrational progressions. ΔG values are in brackets.

	Ne		Ar
v'	C	B	C
0	27 585 (321)	28 330 (297)	26 232 (293)
1	27 905 (320)	28 627 (292)	26 525 (299)
2	28 226 (293)	28 919 (289)	26 824 (298)
3	28 519	29 208	27 122

The corresponding excitation spectrum in an Ar matrix [Fig. 4(a)] starts with a smooth long wing with low intensity and a steep, but still smooth increase ~27 200 cm^{-1}. The wing contains some modulation which can hardly be seen by eye. For demonstration, it has been amplified by differentiation [Fig. 4(a)] and now a clear vibrational progression can be identified in the low intensity wing leading to the energies of the maxima in Table V and the spectroscopic constants in Table I. The assignment of the weak bands to the $C \leftarrow X$ transitions is analogous to the Ne case. Also the steep onset of the $B \leftarrow X$ transitions appears in Fig. 4(a), but no further vibrational progressions can be resolved. Apparently, the homogeneous broadening in Ar is larger than in Ne and it has to exceed 500 cm^{-1} to flatten out the structures up to the observed extent.

A weak broadband appears in the background of the blue wing of the $B^* \rightarrow X$ emission with a longer lifetime. The band can be separated by a time delay of some 100 ns in gated spectra and a central wavelength of 405 nm and a bandwidth of 10 nm [full width at half-maximum (FWHM)] is determined. The band has the same excitation spectrum as the $C \rightarrow A$ emission and is therefore attributed to the $C \rightarrow X$ emission of XeF. The Stokes shift of ~1500 cm^{-1} is of the order of the binding energy of XeF in the ground state.

C. $B^* \rightarrow A'$ emission spectrum in Ar

Near the red wing of the $C \rightarrow A$ emission spectrum in Ar, an additional short lived and broad emission band was identified. The intensity of this band is much weaker than the C–A emission and it was separated by a time window of 10 ns from the longer lived (120 ns) C–A component. The band is centered at 645 nm and has a width of 75 nm (FWHM). The lifetime indicates the B^* state as an upper state and the width shows that one of the repulsive A states is the final state. The $A'(1/2)$ state is favored according to the selection rules. The excitation spectrum of the $B^* \rightarrow A'$ emission is identical to that of the B^*–X emission which definitely proves its assignment to the B^* state.

D. Xe_2F emission and excitation spectrum in Ne

The consideration of contributions of triatomics such as Xe_2F and XeF_2 will be important to explain the different excitation spectra of Figs. 1 and 4. Xe_2F potential surfaces are available from "diatomics in molecules calculations" and the $4\,^2\Gamma \rightarrow 1,2,3\,^2\Gamma$ transitions of this molecule are observed in the gas phase as a broadband at 610±65 nm according to the review of Ref. 1. The emission is shifted to the red in liquid Xe and liquid Ar to 680±30 and 696±32 nm, respectively,[24] and in solid Xe to 775±70 nm.[25] We observed the Xe_2F emission in Ne at 714 nm with a lifetime of 250 ns for Xe concentrations above 0.05%. The excitation spectrum of this band is reproduced in Fig. 5 together with the XeF $C \leftarrow X$ and $B^* \leftarrow X$ excitation spectra and an absorption spectrum from the literature.[2] The $C \leftarrow X$ and $B^* \leftarrow X$ spectra in Fig. 5 are scaled to the intensities in the

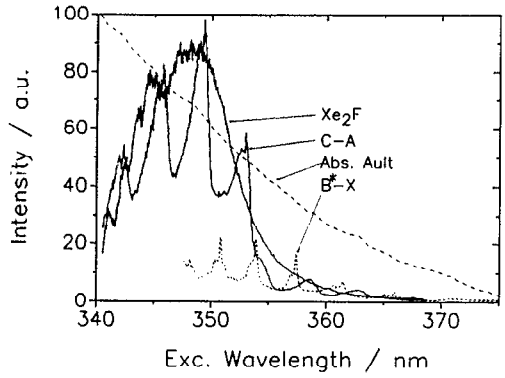

FIG. 5. A comparison of an absorption spectrum of XeF in Ne from Ref. 2 with the B^* and C excitation spectra scaled to the integrated emission intensity and with an amplified Xe_2F (emission at 714 nm) excitation spectrum.

integrated emission spectra. The Xe_2F intensity would be rather small on this scale, and for comparison, it is amplified. The long wavelength part in the Xe_2F excitation spectrum is structureless, which indicates broadening of vibrational bands beyond vibrational spacings. The weak structures in the short wavelength part can hardly be correlated with vibrational bands in the C–X or B^*–X excitation spectra. The broad intensity distribution of the Xe_2F excitation spectrum follows quite closely the envelope of the vibrational progression of the C–X excitation spectrum and definitely not that of the B^*–X excitation spectrum. It seems that the Xe_2F and the C–A emission have similar Franck–Condon distributions in the excitation spectra and the Xe_2F vibrational bands are additionally broadened due to the presence of the second Xe atom.

It would be plausible that the absorption spectrum represents a superposition of the three excitation spectra in Fig. 5. It is remarkable that the structures in the excitation spectra in the region from 340 to 375 nm are not reproduced in the absorption spectrum which is flat. Furthermore, the intensities decrease in all excitation spectra for wavelengths shorter than 345 nm, whereas the absorption spectrum has reached only half of its maximum value and rises up to 330 nm. Obviously the quantum efficiency is strongly reduced for wavelength shorter than 345 nm which is important for an efficient pumping of the laser transitions. The XeF and the Xe_2F excitations are strongly quenched to the repulsive ground state surfaces in the high energy part. A predissociation of Xe_2F due to the crossing of the lowest ionic state with one of the repulsive covalent states was discussed in the gas phase as a cause for the low Xe_2F efficiency.[1]

More information about the composition of the centers involved in the different excitation spectra is contained in the concentration dependencies of the emission bands. Samples with a fixed mole ratio of $Ne:F_2$ of 2000:1 and a Xe content increasing from 1 to 10 and to 40 were grown. A sample with a $Ne|Fe_2|Xe$ ratio of 2000:5:1 was also investigated. The integrated intensities of the B^*–X and the Xe_2F emissions divided by the integrated C–A emission

TABLE VI. Experimental ratios Xe_2F (714 nm)/XeF (C:483 nm) and XeF (B^*:390 nm)/XeF (C:483 nm) of the integrated intensities of the emission bands in the Ne matrix for an excitation wavelength of 353.1 nm are compared with the relative probabilities Xe_2F/XeF and XeF_2/XeF of Xe_2F, XeF_2, and XeF centers according to a statistical distribution after a photolysis cycle (see the text) vs the sample composition.

Ne	Xe	F_2	$Xe_2F(714)$ / XeF(483)	Xe_2F / XeF	XeF(390) / XeF(483)	XeF_2 / XeF
2000	40	1	0.23	0.23	0.4	0.15
	10	1	0.09	0.05	0.45	0.23
	2	1	0.02	0.01	0.33	0.5
	1	1	0.005	0.004	0.17	0.6
	1	5			0.19	1.0

are given in Table VI. The relative Xe_2F contribution rises strongly above Xe concentrations of 0.1%. The B^*/C ratio is essentially constant at low Xe concentration and rises by about a factor of 2 for high Xe concentrations. The increase can be due to a competition of clustering processes which will be discussed later on.

IV. DISCUSSION

The $B^*\leftarrow X$, $C\leftarrow X$, and Xe_2F excitation and the $B^*\rightarrow X$, B^*–A', C–A and Xe_2F emission spectra were assigned in Sec. III. All investigations agree that the vibrational relaxation is fast in the electronic states on the time scale of the exciting pulse lengths (10 ns) and radiative lifetimes (5–120 ns). In an earlier paper, the relaxation in the $v'=0$–4 levels of the B state was treated in more detail[21] and it was shown that the relaxation is faster than 0.01 ns for $v'\geqslant 4$, and only from $v'=1$ to $v'=0$ longer relaxation times between 0.1–1 ns appear. If we assume that all the observed B^* and C emissions originate from the same type of XeF molecules, then we would predict according to this information that the $v=0$ states of B^* and C are populated through a cascade of intramolecular vibrational relaxation and B^*–C internal conversion processes with a branching ratio which is reflected in the relative intensities of the B^* and C emissions. The $B^*(v'=0)$ and $C(v'=0)$ levels do not communicate because they decay with their very different individual lifetimes and the $C(v'=0)$ lifetimes do not show up as rise times, too. Therefore, these internal conversion processes would be expected in the vibrational manifolds of the nested B^* and C potential curves with $v'\geqslant 1$. In this case, the excitation spectra of the B^* and C emissions should contain the mutual B^* and C vibrational progression, but if we compare the excitation spectra of C emission (Fig. 4) with those of B^* emission (Fig. 1), then all the structured vibrational bands from Fig. 1 are missing in Fig. 4, and the broadbands, especially of Fig. 4(b) are absent in Fig. 1(b). It is less evident, but the same holds according to a careful comparison even for the soft modulations from Fig. 4(a). Thus the B and C state excitations from Fig. 4 do not contribute to the B^*–X emission shown in Fig. 1 and vice versa. Therefore, the B^* and C state emissions have to originate from two different types of XeF molecules. These two types of molecules do not exchange excited state pop-

ulations and the spectroscopic properties are significantly different as is illustrated by the very different excitation spectra of Figs. 1 and 4. Thus our data prove the original assignment[3] of the B^* and C emissions to two types of species. A larger C/B^* intensity ratio was observed in Ref. 3 for an increase in concentration of the F delivering compound. In our experiments, the C/B^* intensity ratio increases with the F_2 photolysis time in Ar because the B^* intensity saturates earlier than the C emission with irradiation time. In addition, XeF populations can be built up by F_2 photolysis, then partly destroyed by XeF dissociation in the C–A transition and again regenerated by thermal and photolysis cycles[11,21] with variations in the B^* and C intensity ratios. From all these observations, it follows that two types of XeF molecules are present and each one gives either $B^* \rightarrow X$ or $C \rightarrow A$ emission.

A. $C \rightarrow A$ emitting species

A comparison of the vibrational parameters of the B and C states in Ne with those in the gas phase (Table I) shows that they are very similar. The difference is only about 5%, which is close to the accuracy limit of the matrix values, with the matrix values being smaller than the gas phase values. These observations are in full accord with the general trends observed for vibrational quanta of molecules in rare gas matrices[26] and further support the assignment. The larger ω_e of the C state as compared to B is preserved in the matrix, also preserved is the trend in anharmonicities $\omega_e x_e$ (Table I). The T_e values demonstrate that the relative ordering is conserved in the matrix and the C state lies about 800 cm^{-1} below the B state. Thus the B state is situated about two vibrational quanta above the C state and can be efficiently quenched to the C state. The small C state rise time of the order of 0.01 ns gives a B to C intensity ratio of less than 0.002.

In going from the Ne to Ar matrix, the agreement with respect to the vibrational quanta, the ordering of the states, and the quenching of the B state emission is reproduced, but the spectroscopic data are less accurate due to the only weakly resolved vibrational progressions. Here, a comparison of the matrix shifts of the T_e values is instructive. Qualitatively, the expected stronger red shift in Ar due to the larger polarizability is reflected in the data. Also the larger dipole moment of the B state because of the greater R_e leads to an enhanced red shift compared to the C state in the Ne matrix, but a quantitative estimate for the shift ΔE with the dielectric constant ϵ of the matrix, the change of the dipole moment $\Delta\mu$ in the transition, and the diameter d of the cavity from[27]

$$\Delta E = -8(\epsilon-1)\Delta\mu^2/(2\epsilon+1)d^2$$

is not obvious.

Assuming that d is determined by the large XeF, then the ratio of the ΔE values from Ar to Ne follows only from the different ϵ values since $\Delta\mu$ is the same. This ratio should amount to 1.9, whereas the observed ratios for B and C are of the order of 3 to 4. On the other hand, d values of 7.9 and 6.4 Å are obtained if we take the experimental shifts of 500 and 1800 cm^{-1}, the ϵ values of 1.3 and 1.69 for Ne and Ar, respectively, and the $\Delta\mu$ value of 8 D for the R_e of the XeF ground state. The Ar value is closer to an estimated size of 5.1 Å for the XeF molecule from the bond length (2.29 Å) and the atomic radii of 2.17 and 0.64 Å for Xe and F, respectively, compared to the very large Ne value.

Now it is interesting to check to which XeF species the D excitation and emission belongs and if it shows a similar trend too. The vibrational bands in the excitation spectra in Ne have a width of 180 cm^{-1} FWHM,[3] and in Ar, they are broadened furthermore and merge to a continuum[3] which is equivalent to the spectra in Fig. 4 for the C emitting species. The ω_e values are close to the gas phase value (Table II) and the matrix shifts of the T_e values of 459 and 2000 cm^{-1} (Table I) are also similar to the C emitting species. Thus the D–X and C–A emissions originate both from the same species, and for this species, the T_e values of the three states B, C, and D show a similar strong increase in matrix shift from Ne to Ar by a factor of 3–4. The polarization model has been applied successfully in several cases[25,28] and an agreement within typically 0.1–0.05 eV was achieved. The overall matrix shift in Ne is only about 0.06 eV and lies within the limits of predictability of the model. Probably for a quantitative treatment of the overall small matrix shift in Ne, contributions from the pair potentials cannot be neglected anymore.

B. $B^* \rightarrow X$ emitting species

The following observations are characteristic for the B^*–X emitting species:

(i) the B^*–X transition energy is reduced in Ar and Ne by 2600–2200 cm^{-1} compared to B–X;

(ii) no C emission has been detected and no C progression below the B progression has been identified in the excitation spectra. This indicates that C^* lies above B^* in this species and is completely quenched to B^*. It also means that the C state energy is reduced less than that of B;

(iii) no D–X emission shows up in this site;

(iv) ω_e of the B state is enlarged from 309 cm^{-1} in the gas to 446 cm^{-1} in solid Ne, i.e., by 30%, and also the anharmonicity is larger;

(v) the irregular vibrational spacings of the maxima in the B^* emission, the changes in line shapes in Ar, and the narrow Franck–Condon envelope in Ne are inconsistent with a diatomic molecule.

An identification of the B^* emitting species has to account for these significant deviations from the gas phase and C emitting XeF molecule and for the composition from Xe and F as well as for the general similarity in electronic structure and selection rules to XeF. The differences in ω_e are too large to attribute the C and B^* emitting centers to XeF in different lattice sites, e.g., single and double vacancies, since site effects on vibrational frequencies are typically only of the order of some percent.[26] If such a strong effect would be acceptable, then it should vary strongly from Ar to Ne due to the change in lattice constants and pair potentials, but this is not the case. Formation of triatomic complexes in the excited states like

$(NeXe)^+F^-$ and $(ArXe)^+F^-$ can play a role. Due to the very large difference in the ionization energies of Ar and Ne, again a strong change of the effects with the matrix would be expected. The dissociation energy, e.g., decreases from 0.176 eV for the $(ArXe)^+$ ground state dimer ion to 0.041 eV for $(NeXe)^+$ (Refs. 29 and 30) and $(ArF)^-$ and $(NeF)^-$ should show a similar trend.[31] This effect can contribute to the shifts of the T_e values, but should not dominate the changes in ω_e values.

Formation of centers as Xe_2F, XeF_2, and $(XeF)_2$ by clustering is suggested by the different concentration dependencies of the *C* and *B** intensities. The envelope of the excitation spectrum of the Xe_2F emission in Fig. 5 is similar to that of the *C* emission. A different orientation of the second Xe atom to the XeF axis in the ground state can be responsible for a strong inhomogenous broadening in excitation and can explain the loss in vibrational structure. Therefore it is not likely that the *B* emitting species belongs to a Xe_2F center. In addition, it would be necessary to postulate a blocking of the relaxation to the minimum in the $Xe_2^+F^-$ potential surface for this special *B** emitting Xe_2F center. Thus XeF_2 and $(XeF)_2$ remain as candidates. Referring to the concentration dependence in Table VI, we assume that the original sample contains Xe, Xe_2, XeF_2, and $(XeF)_2$ centers according to the statistical distribution given by the concentrations. Next we assume that the F atoms generated in the F_2 photolysis form XeF, Xe_2F, and XeF_2 with statistically disturbed Xe, Xe_2, and XeF centers because the hot F atoms are able to sample a large volume.[15–20] This evaluation is not self-consistent and ignores dissociation of the generated XeF, XeF_2 and $(XeF)_2$. It serves only for an estimate because also the statistical distributions could be questioned. The comparison in Table VI shows a quite similar increase in the observed $Xe_2F(714)/XeF(483)$ intensity ratio with the predicted Xe_2F/XeF concentration ratio for increasing Xe concentration, which supports our model. In accepting this agreement, we exclude already an assignment of the *B** center to special Xe_2F or $(XeF)_2$ centers because the quite large B^*/C ratio at small Xe concentrations below 0.05% would require a sufficient concentration of original Xe_2 centers, which is in contradiction to the low Xe_2F intensity. The evaluation yields for all samples a rather large XeF_2/XeF ratio growing from 0.15 to 1 with reduction in Xe concentration. The experimental B^*/C ratio varies between 0.4 and 0.17 and is of the same order of magnitude. The model overestimates the XeF_2 content by neglecting its dissociation. The assignment of the *B** emitting species to a XeF_2 center is therefore consistent with the experimental concentration dependence.

Recent investigations confirm a close relationship of *B** emission quenching and XeF_2 production in liquid Ar, thus supporting the assignment of *B** to XeF_2. The stable XeF_2 molecule with a linear F–Xe–F structure is formed in liquid Ar and suppresses the amplified spontaneous emission of XeF.[32] Buildup of XeF_2 was not observed in solid Ar and Ne despite intense pumping of the crystals in laser applications,[12–14] and only a long term fading of the laser efficiency could be due to slow XeF_2 production. Table VI suggests that F atoms come close to XeF centers also in the crystals. XeF_2 production seems to be inhibited by steric hindrance or a combination of barriers and relaxation processes which are specific to the crystalline state. The electronic states of the stable XeF_2 compound lie at energies far above the *B** excitation energies. Thus the *B** emission has to be attributed to a precursor of the XeF_2 molecule, which in the liquid state has comparable chances to radiate or to bind and which in crystalline matrices decays predominately radiatively. Goodman and Brus[3] arrived at a similar conclusion by studying the *B** intensity for different F atoms delivering parent molecules.

These centers seem to be an interesting and challenging candidate for a treatment by a combination of the "diatomic in molecules method" with molecular dynamics calculations.[33] Information concerning the nested *C** state and its relaxation processes is available from time resolved experiments.[21] The fine structure in the vibrational bands (Fig. 1, Table III) delivers fingerprints for the internal dynamics of the center and the interaction with the matrix. A high frequency mode of 60 cm^{-1} shows up in Ar and Ne. It is close to the maximum of the phonon density in the matrices and is probably related to a coupling of the center to the lattice. The smaller frequencies of 30 cm^{-1} in Ne and 15 cm^{-1} in Ar seem to be typical for the center and librations or internal vibrations can be involved. Excitation spectra for a large family of rare gas–halogen charge transfer states are available. It is remarkable that the *B** excitation spectra in Ar and Ne are the only examples with well-resolved fine structure progressions. Broadening by coupling to the lattice has to be weaker in this case despite the larger number of degrees of freedom and this fact should be reflected in the structure of the center. A Xe^+F^- charge transfer excitation causes a shrinkage of the Xe radius to that of Xe^+ by some tenth of an Ångstrom and a similar growth of F to F^-, thus the overall changes of size are small. The shift of the center of the XeF molecule initiates a push by the surrounding matrix to accommodate in the new equilibrium position, resulting in vibrations, i.e., broadening by electron–phonon coupling. The weak broadening in the *B** state is consistent with a linear and symmetric charge transfer structure F^-–Xe^+–F^- with fractional or delocalized F^- charges. The center remains in Xe for the ground and excited states and displacements are reduced. This charge transfer state dressed by the matrix polarization could be a precursor state lying energetically above the stable covalently bound ground state of XeF_2 and relaxing to XeF_2 in liquid Ar, but predissociating to XeF+F in solid Ar and Ne.

C. Potential surfaces for the *B*, *C*, and *B** states

To support a modeling, we try to represent the complex multidimensional potential surfaces by empirical pair potentials derived from the spectroscopic constants. It is convenient to start with Morse potentials because of the analytical simplicity. The parameters D_e (cm^{-1}) and $\beta(Å^{-1})$ for the potential

$$U = T_e + D_e\{1 - \exp[-\beta(r - r_e)]\}^2$$

TABLE VII. Parameters for a representation of the potentials for the *B*, *C*, and *B** states in Ne and for *B** in Ar matrices by a Morse potential or a Rittner potential. For definitions, see the text.

	Ne			Ar
	B	*C*	*B**	*B**
Morse				
$T_e(\mathrm{cm}^{-1})$	28 303	27 544	26 071	24 566
$r_e(\text{Å})$	2.57	2.45	2.46	2.46
$D_e(\mathrm{cm}^{-1})$	11 325	9 075	3 527	5 993
$\beta(\text{Å}^{-1})$	1.404	1.719	3.727	2.718
Rittner				
$a(\mathrm{cm}^{-1})$	61 343	63 415	48 626	52 978
$b(\mathrm{cm}^{-1})$	3.707×10^{7}	3.059×10^{7}	1.495×10^{15}	6.512×10^{11}
$\beta(\text{Å}^{-1})$	3.405	3.365	11.1	8.09
ϵ	1.3	1.3	2	1.69
$C_4(\text{Å}^4\mathrm{cm}^{-1})$	1.809×10^{5}	1.809×10^{5}	0	0
$\omega_e x_e(\mathrm{cm}^{-1})$	1.83	1.9	12.9	8.0
$D_R(\mathrm{cm}^{-1})$	33 040	35 871	22 555	28 412

were derived from the spectroscopic constants ω_e (cm^{-1}) and $\omega_e x_e$ (cm^{-1}) (Table I) by

$$D_e=\omega_e^2/4(\omega_e x_e)$$

and

$$\beta=0.243\,54\sqrt{\mu_r\omega_e x_e}$$

with the reduced mass $\mu_r=16.6$ (a.u.). For *C* and *B**, r_e was estimated from the intensity maximum of the vibrational progression in the excitation spectra and for *B* from that in absorption[2] assuming a ground state bond length of 2.29 Å from the gas phase. These values are collected in Table VII for *B*, *C*, and *B** in Ne and for *B** in Ar. The well depths D_e of about 10.000 cm^{-1} are significantly too low, which is not surprising because the Morse potential is not appropriate to describe the softly rising Coulomb part in the Xe^+F^- ionic bonding. Therefore, also a representation by a Rittner potential truncated at the r^{-4} term is provided[4]

$$U=a+b\exp(-\beta r)-e^2/\epsilon r-C_4/r^4.$$

The dielectric shielding was included in the Coulomb and C_4 terms by the dielectric constant ϵ of the matrix and the reduction of ϵ for small r values was ignored. The β, a, and b parameters were calculated from the experimental ω_e and T_e with r_e from the previous Morse potential by

$$\beta=(0.03\mu_r\mu\omega_e^2r_e^2+2e^2/\epsilon r_e+20C_4/r_e^4)/(e^2/\epsilon+4C_4/r_e^3),$$

$$a=T_e+e^2(1-1/\beta r_e)/\epsilon r_e+4C_4(1/4-1/\beta r_e)/r_e^4,$$

$$b=(e^2/\epsilon r_e+C_4/r_e^4+T_e-a)\exp(\beta r_e)$$

using the F^- and Xe^+ polarizabilities α_1 and α_2 for C_4

$$C_4=(\alpha_1+\alpha_2)e^2/2\epsilon.$$

The values for *B* and *C* in Ne are listed in Table VII and the potentials are displayed in Fig. 6. The resulting a values of 61 343 and 63 415 cm^{-1} represent the Xe^++F^- energies for $r\to\infty$ and should correspond in the matrix to

$$a=I_g+E_A+P_++P_-+D_0$$

with the gas phase Xe ionization energy I_g; the electron affinity E_A of F; the polarization energies P_+ of Xe and P_- of F^- of the Ne matrix; and the ground state well depth $D_0\approx1495$ cm^{-1}. *B* and *C* dissociate to the same ionic states and it is satisfying that the resulting a values agree within 2000 cm^{-1}. The a value in Ne is smaller than the gas phase value of 71 580 in agreement with a solvation of the ions. The polarizations energies P_++P_- of about 9000 cm^{-1} or 1.2 eV show the expected order of magnitude and a more quantitative discussion would require a better knowledge of P_- in Ne. The essential point is that the Rittner potential provides very reasonable well depths $D_R=a-T_e$ of 33 040 and 35 871 cm^{-1} for *B* and *C*, respectively, compared to the much too low values from the Morse potentials of the order of 10 000 cm^{-1}. The comparison of the predicted and measured anharmonicities provides a further check. $\omega_e x_e$ (cm^{-1}) follows (Table VII) for the Rittner potential from

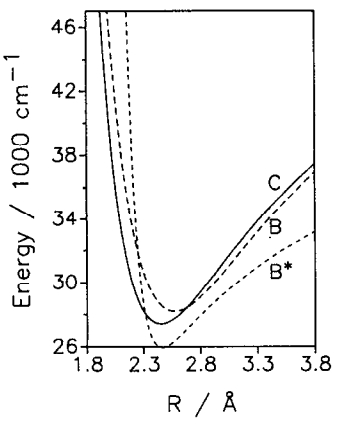

FIG. 6. Rittner potentials for the *B*, *C*, and *B** states in the Ne matrix fitted to the spectroscopic constants of Table VII with energies of 61 343, 63 415, and 48 626 cm^{-1} for $r\to\infty$.

$$\omega_e x_e = \left\{ \frac{5}{3} \left[\frac{(t^2-6)+2(\alpha_1+\alpha_2)(t^2-30)/r_e^3}{t-2+2(\alpha_1+\alpha_2)(t-5)/r_e^3} \right]^2 - \frac{(t^3-24+2(\alpha_1\alpha_2)(t^3-210)/r_e^3}{t-2+2(\alpha_1+\alpha_2)(t-5)/r_e^3} \right\} \frac{2.1078}{\mu r_e^2}$$

with the abbreviation $t=\beta r_e$. The predicted values of 1.8 and 1.9 cm^{-1} agree within the accuracy with the measured values of 2 and 3 cm^{-1} for B and C, respectively. A good fit for B^* in Ar and Ne could only be obtained by taking $C_4=0$ and by increasing ϵ to the values given in Table VII. An explanation can be the complex structure which leads to deviations from a potential between two charged and polarizable particles. The resulting Rittner constants are collected in Table VII and the potential for B^* in Ne is plotted in Fig. 6.

ACKNOWLEDGMENTS

This work was supported by the Deutsche Forschungsgemeinschaft via the Sonderforschungsbereich 337, by a grant from the U.S. National Science Foundation ECS-8914321, and in part by a contract from the U.S. Air Force Phillips Laboratory S04611-90-K-0035. G. S. Fellow of The Comission of European Communities, acknowledges the CEC support, contract 791, during his stay in Berlin.

[1] D. L. Huestis, G. Marowsky, and F. K. Tittel, in *Excimer Lasers*, 2nd ed., edited by Ch. K. Rhodes (Springer, Berlin, 1984), p. 181 ff.
[2] B. S. Ault and L. Andrews, J. Chem. Phys. **65**, 4192 (1976).
[3] J. Goodman and L. E. Brus, J. Chem. Phys. **65**, 3808 (1976).
[4] J. Tellinghuisen, P. C. Tellinghuisen, G. C. Tisone, J. M. Hoffmann, and A. K. Hays, J. Chem. Phys. **68**, 5177 (1978).
[5] P. C. Tellinghuisen, J. Tellinghuisen, J. A. Coxon, J. E. Velazco, and D. W. Setser, J. Chem. Phys. **68**, 5187 (1978).
[6] H. Helm, D. L. Huestis, M. J. Dyer, and D. C. Lorents, J. Chem. Phys. **79**, 3220 (1983).
[7] P. J. Hay and T. H. Dunning, J. Chem. Phys. **69**, 2209 (1978).
[8] N. Schwentner and V. A. Apkarian, Chem. Phys. Lett. **154**, 413 (1989).
[9] A. I. Katz, J. Feld, and V. A. Apkarian, Opt. Lett. **14**, 441 (1989).
[10] H. Kunttu, W. G. Lawrence, and V. A. Apkarian, J. Chem. Phys. **94**, 1692 (1991).
[11] G. Zerza, F. Knopp, R. Kometer, and G. Sliwinski, SPIE **1410**, 202 (1981).
[12] G. Zerza, G. Sliwinski, and N. Schwentner, Appl. Phys. A **54**, 106 (1992).
[13] G. Zerza, G. Sliwinski, and N. Schwentner, Appl. Phys. B **55**, 331 (1992).
[14] G. Zerza, G. Sliwinski, and N. Schwentner, Appl. Phys. A **56**, 156 (1993).
[15] H. Kunttu and V. A. Apkarian, Chem. Phys. Lett. **171**, 423 (1990).
[16] R. Alimi, R. B. Gerber, and V. A. Apkarian, J. Chem. Phys. **92**, 3551 (1990).
[17] J. Feld, W. Kunttu, and V. A. Apkarian, J. Chem. Phys. **93**, 1009 (1990).
[18] H. Kunttu, J. Feld, R. Alimi, A. Becker, and V. A. Apkarian, J. Chem. Phys. **92**, 4856 (1990).
[19] H. Kunttu, E. Sekreta, and V. A. Apkarian, J. Chem. Phys. **94**, 7819 (1991).
[20] G. Zerza, R. Kometer, G. Sliwinski, and N. Schwentner, J. Lumin. **48/49** (1991).
[21] G. J. Hoffman, D. Imre, R. Zadoyan, N. Schwentner, and V. A. Apkarian, J. Chem. Phys. **98**, 9233 (1993).
[22] E. Schuberth, M. Creuzburg, and W. Müller-Lierheim, Phys. Status Solidi B **76**, 301 (1976).
[23] V. Aquilanti, E. Luzzatti, F. Pirani, and G. G. Volpi, J. Chem. Phys. **89**, 6165 (1988).
[24] H. Jara, H. Pummer, and C. K. Rhodes, Phys. Rev. B **30**, 1 (1984).
[25] M. E. Fajardo and V. A. Apkarian, J. Chem. Phys. **85**, 5660 (1986).
[26] M. E. Jacox, J. Phys. Chem. Ref. Data **13**, 945 (1984).
[27] D. C. McKean, Spectrochim. Acta Part A **23**, 2405 (1967).
[28] M. Kraas and P. Grütler, Chem. Phys. Lett. **183**, 264 (1991); **187**, 527 (1991).
[29] P. M. Dehmer and S. T. Pratt, J. Chem. Phys. **77**, 4804 (1982); S. T. Pratt and P. M. Oehmer, *ibid.* **76**, 3433 (1982).
[30] D. Hausamann and H. Morgner, Mol. Phys. **54**, 1085 (1985).
[31] M. Hill and V. A. Apkarian (to be published).
[32] M. Shahidi, H. Jara, H. Pummer, H. Egger, and C. K. Rhodes, Opt. Lett. **10**, 448 (1985).
[33] I. H. Gersonde and H. Gabriel, J. Chem. Phys. **98**, 2094 (1993).